Article

Experimental Validation of the Neurotrophic Factor-α1 Binding Site on the Serotonin Receptor 1E (HTR1E) Responsible for β-Arrestin Activation and Subsequent Neuroprotection

Xuyu Yang,[#] Joo-Youn Lee,[#] Soo-Kyung Kim, Y. Peng Loh,* and William A. Goddard, III*
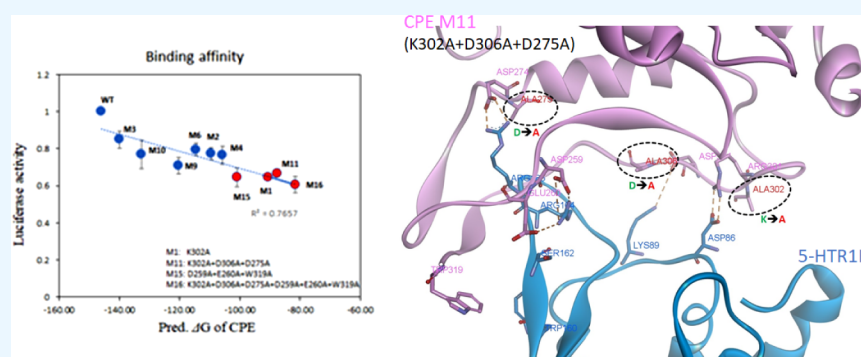
Read Online

ACCESS | Metrics & More | Article Recommendations | SI Supporting Information

ABSTRACT: Stress, such as neuroexcitotoxicity and oxidative stress, as well as traumatic brain injury, will result in neurodegeneration. Deciphering the mechanisms underlying neuronal cell death will facilitate the development of drugs that can promote neuronal survival and repair through neurogenesis. Many growth and trophic factors, including transforming growth factors (TGFs), insulin-like growth factors (IGFs), epidermal growth factor (EGF), fibroblast growth factor 2 (FGF2), and brain-derived neurotrophic factor (BDNF), are known to play a role in neuroprotection and neurogenesis. Neurotrophic factor-α1 (NF-α1), also known as carboxypeptidase E (CPE), has been shown experimentally to have neuroprotective activity, acting extracellularly, independent of its intracellular enzymatic function in prohormone processing. We previously reported experiments and molecular dynamics (MD) simulations showing that a 200 amino acid segment of NF-α1/CPE interacts with the serotonin receptor 1E (HTR1E) to protect human neurons against oxidative and neuroexcitotoxic stress via β-arrestin and extracellular signal-regulated kinase (ERK) signaling. We report here validation of our previously predicted binding site with a series of 16 carboxypeptidase E (CPE) mutants, identifying 3 mutants that substantially decrease the binding to HTR1E. We then carried out pERK studies to show that these 3 mutants also dramatically reduce β-arrestin activation. This was followed by MD simulations of 8 selected mutants, finding that the same 3 most dramatically reduced binding of the mutated CPE to 5-HTR1E. Then, we examined the binding of β-arrestin to these 3 (after phosphorylating the intracellular Ser and Thr) and found that the predicted binding decreased dramatically. Then, we examined the predicted activation of the β-arrestin by these 3 and found a dramatic decrease, just as in the pERK experiments. We consider that these experiments and simulations fully validate the predicted binding site for CPE, identifying the key amino acid residues critical for binding and biological activity. This provides the target for experiments and *in silico* computational screening to identify small molecules to replace the CPE protein as novel drugs to protect human neurons against oxidative/neuroexcitotoxic stress via β-arrestin/ERK signaling.

INTRODUCTION

Neurodegenerative diseases such as Alzheimer's disease and Parkinson's disease have become prevalent globally in part due to an increased aging population. Hallmarks of these diseases are characterized by degeneration of the nervous system, including apoptosis of nerve cells, activation of microglial cells, deposition of amyloid protein aggregates, and tau tangles in the brain, resulting in neuroinflammation and cognitive dysfunction.[1] Neuronal cell death is often caused by environmental and oxidative stress and neurotoxicity. There is a growing need for therapeutics that can treat neurodegeneration. Under-

standing the mechanisms that can protect against neuronal cell death will facilitate the development of therapeutics that can mitigate these challenges. Indeed, many growth and trophic
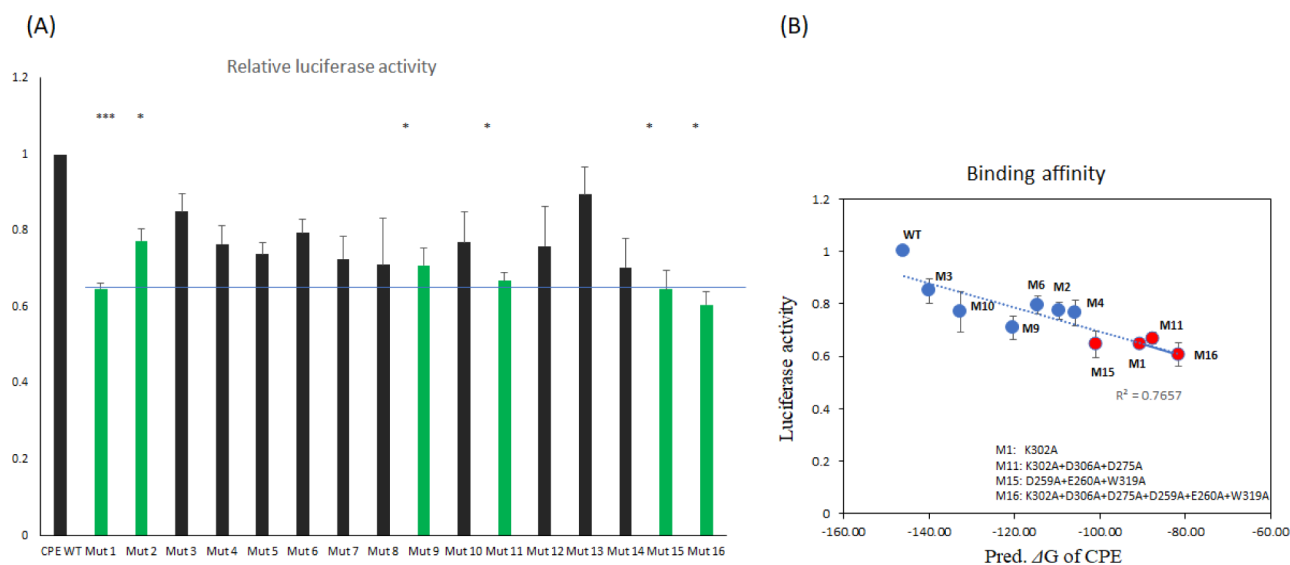
Figure 1. Experimental and calculated binding affinity for various mutants. (A) Effect of CPE mutants on 5-HTR1E−CPE binding affinity. The Presto-Tango reporter system was used to measure the binding affinity between the CPE mutants and 5-HTR1E. Each of the 16 CPE mutants was coexpressed with 5-HTR1E in HTLA cells, and luciferase activity was measured using whole cell extracts from transfected cells. Renilla luciferase was used as internal control to normalize expression efficacy. The bar graph shows the relative luciferase activity normalized against WT-CPE. Student's t-test was used for statistical analysis. Mutants: M1: K302A, M2: D259A, M3: D259N, M4: D275A, M5: D275N, M6: D306A, M7: D306N, M8: 260A, M9: E260Q, M10: W319A, M11: K302A + D306A + D275A, M12: D259A + E260A, M13: K302A + D259A + E260A, M14: K302A + D306A + W319A, M15: D259A + E260A + W319A, M16: K302A + D306A + D275A + D259A + E260A + W319A. Values mean ± SEM ($N = 5$). ***$p < 0.001$, *$p < 0.05$. (B) Comparison of the predicted binding free energies (ΔG) using MD simulation trajectories with experimental luciferase activity. The predicted binding free energies of M1, M11, M15, and M16 were highly correlated to the experimental luciferase activity. The red circle indicates a significant alteration in the binding affinity as observed in luciferase tests.

factors, such as transforming growth factors (TGFs), insulin-like growth factors (IGFs), epidermal growth factor (EGF), fibroblast growth factor 2 (FGF2), and brain-derived neurotrophic factor (BDNF), are known to play a role in neuroprotection.[2−4] Neurotrophic factor-1 (NF-α1), also known as carboxypeptidase E (CPE), was originally identified as a prohormone processing enzyme. Multiple lines of experimental evidence have shown that CPE possesses neuroprotective activity acting extracellularly, independent of its intracellular enzymatic function.[5−7] Moreover, studies have shown that adeno-associated virus (AAV)-NF-α1/CPE injected bilaterally into the hippocampus of Alzheimer disease mice (3xTg-AD) prevented neurodegeneration, amyloidosis, tau hyperphosphorylation, and cognitive dysfunction in these animals.[8] It has also been reported that injection of two agomirs into the hippocampus of 9 month old APP/PS1 AD mice that up-regulated CPE expression mitigated AD pathology in these mice.[9] Recently, we reported experiments and molecular dynamics (MD) simulations, showing that a 200 amino acid segment of NF-α1/CPE (150−350 aa) interacts with the serotonin receptor 1E (5-HTR1E), a G protein-coupled receptor (GPCR) expressed in humans and primates but not in mice.[10] We showed that the central 200 amino acid part of NF-α1/CPE mediates the binding to 5-HTR1E, and we carried out 1.5 μs of MD to predict the binding site of CPE to the extracellular loops of 5-HTR1E.[11] Then, we phosphorylated Ser and Thr in the intracellular loops (ICLs) computationally and predicted the binding of β-arrestin, showing that it is activated by CPE. The predicted binding site involved six polar interactions with the extracellular loops (ECLs), ECL1, ECL2, and ECL3 of 5-HTR1E. The predicted interactions were as follows: four salt bridges K302−D86 (ECL1), D306−K89 (ECL1), D275−R165 (ECL2), D259−R164 (ECL2);

one hydrogen bond: E260−S162 (ECL2); and an aromatic interaction: W319−W160 (ECL2). Furthermore, after phosphorylating the Ser and Thr of the C-terminal tail and intracellular loop 3 (ICL3) of NF-α1/CPE−5-HTR1E, our MD predicted that β-arrestin1 forms numerous salt bridges and hydrogen bonds to ICL2 and ICL3, leading to the activation of β-arrestin1. Indeed, our experiments showed that NF-α1/CPE−5-HTR1E activates a signal transduction mechanism leading to cell survival that protects human neurons against oxidative/neuroexcitotoxic stress via β-arrestin/ERK signaling.[11]

The current work aims at validating the binding site predicted previously[11] by measuring the binding and activation experimentally for various mutations of the residues in NF-α1/CPE predicted to bind to the binding site. We report here mutation and binding experiments to test the previously reported binding site as well as new MD simulations and binding calculations on the same mutations to verify the new experiments. We then correlated changes in the MD of the mutants with experimental deficits in neuroprotection and extracellular signal-regulated kinase (ERK) activation to identify the most critical amino acid residues involved in the interaction between CPE and 5-HTR1E to mediate function. These studies confirm the predicted binding site and uncover specific amino acids in the interaction with HTR1E that are important for biological activity, setting the stage for *in silico* virtual screening to identify small molecules to protect human neurons against oxidative/neuroexcitotoxic stress via β-arrestin/ERK signaling.

■ RESULTS AND DISCUSSION

Mutations of Specific Amino Acids in CPE Affect Its Binding Affinity to 5-HTR1E. To validate the predicted sites

responsible for the CPE/HTR1E interaction from our previous report[9] and to check whether there are synergistic or antagonistic effects among these sites that affect the binding between CPE and HTR1E, we constructed 16 plasmids expressing individual CPE mutations or mutation combinations targeted to these sites (DNA constructs, supplementary). We verified that these constructs were expressed and secreted efficiently from HTLA cells. Western blot analysis indicated that each of the CPE mutant constructs was expressed and secreted at a similar level as wild type (WT) CPE from the cells (Figure S1). We coexpressed these CPE mutants along with 5-HTR1E in the Presto-Tango system reporter cells, HTLA, and measured luminescence to reflect the binding affinity between CPE mutants and 5-HTR1E (Figure 1A,B). Our luciferase tests indicated that the binding affinity changed dramatically (as indicated by the lower luciferase activity) for six mutant CPE constructs (Figure 1A):

- the single mutation CPE M1 (K302A) decreased binding to 64.7%,
- the single mutation CPE M2 (D259A) decreased binding to 77.2%,
- the single mutation CPE M9 (E260Q) decreased binding to 70.8%,

and three combinations of mutations

- CPE M11 (K302A + D306A + D275A) decreased binding to 66.8%,
- CPE M15 (D259A + E260A + W319A) decreased binding to 64.5%, and
- CPE M16 (K302A + D306A + D275A + D259A + E260A + W319A) decreased binding to 60.5%.

Among the single mutations, mutant K302A showed the lowest binding affinity, although the combined mutations M11, M15, and M16 attenuated the binding affinity to 66.8%, 64.5%, and 60.5%, respectively. This decrease is similar to that caused by the single mutation M1, suggesting that the other sites D306, D275, D259A, E260, and W319A may not be as important as site K302 in terms of binding to HTR1E. In addition, these sites might not generate a synergistic effect for the binding between CPE and HTR1E. According to our screening data, we hypothesized that CPE site K302 could be the most important amino acid for the interaction between CPE and 5-HTR1E.

To compare these experiments, we conducted 100 ns MD simulations for all mutants. [All parameters for the MD simulation and for the MM-GBSA method are depicted in detail in Materials and Methods.] We then calculated the change in the predicted CPE binding energy, as shown in Table 1. Except for M1 (K302A), M11 (K302A + D306A + D275A), M15 (D259A + E260A + W319A), and M16 (K302A + D306A + D275A + D259A + E260A + W319A), the experimental error bars are large and include the possibility of no effect. We focus on M1 (K302A), M11 (K302A + D306A + D275A), and M15 (D259A + E260A + W319A), for which there definitely is an experimental decrease. Indeed, our new MD calculations predict that these four lead to the largest decrease in binding of the mutants. Since M16 (K302A + D306A + D275A + D259A + E260A + W319A) mutation sites are covered by the other combinations, and due to the complexity of 6 mutation sites, we have not included them for further MD simulation studies.

For M1 (K302A), the predicted binding is only 62% of that for WT, which is in excellent agreement with the experimental

Table 1. Predicted Binding Free Energies of the 10 CPE Mutants Based on the Molecular Dynamics (MD) by MM-GBSA for 5-HTR1E−CPE Mutant Complexes, Compared to the Luciferase Activity (Lower Ratio → Less Binding)[a]

name	mutation	predicted ΔG of binding for mutated CPE	relative predicted ΔG (fraction) of binding	ratio experimental luciferase activity (SEM)[b]
WT		−145.94	1	1
M3	D259N	−139.92	0.96	0.85 ± 0.05
M6	D306A	−114.61	0.79	0.79 ± 0.03
M10	W319A	−132.52	0.91	0.77 ± 0.08
M2	D259A	−109.52	0.75	0.77 ± 0.03
M4	D275A	−105.59	0.72	0.76 ± 0.05
M9	E260Q	−120.21	0.82	0.71 ± 0.04
M11	**K302A + D306A + D275A**	**−87.62**	**0.60**	**0.67 ± 0.02**
M15	**D259A + E260A + W319A**	**−101.06**	**0.69**	**0.65 ± 0.01**
M1	**K302A**	**−90.56**	**0.62**	**0.65 ± 0.05**
M16	**K302A+D306A +D275A +D259A +E260A +W319A**	**−81.51**	**0.56**	**0.61 ± 0.04**

[a]In bold face are the four mutants, M1 (K302A), M11 (K302A + D306A + D275A), M15 (D259A + E260A + W319A), and M16 (K302A + D306A + D275A + D259A + E260A + W319A), considered to demonstrate an experimentally significant decrease in experimental activity [b]Results are expressed as mean ± SEM for each mutants.

decrease in binding to 64.7%. Figure 2A compares the structural changes in 5-HTR1E for the K302A mutant to that of WT. The most dramatic change is that TM6 moves away from TM5 toward the outside by 6.48 Å farther than for WT (measuring the distance between both I313 Cα), moving the EC3 loop with it. This dramatic repositioning of TM6 leads to a decreased level of binding of HTR1E to the K302A mutant CPE.

Figure 2B compares the structures for WT with that of the M11 (K302A + D306A + D275A) mutant. This triple combination mutant moves TM6 away from TM5 by 3.89 Å compared to WT, 2.59 Å less than for the M1 (K302A) mutant. Table 1 shows that the predicted binding energy for M11 (K302A + D306A + D275A) is 60%, similar to the experimental decrease in binding to 66%, and close to the predicted decrease of 60% for the M1 (K302A) single mutant.

Figure 2C compares the structures for WT with that of the M15 (D259A+E260A+W319A) mutant. In this case, the conformations of both TM6 and TM7 change, moving 3.74 and 3.12 Å [measuring the distance between both Cα of S323] farther from TM5 compared to WT. Table 1 shows that the predicted binding energy for M15 (D259A + E260A + W319A) is 69%, which is the highest among the four mutants with the poorest binding. This can be compared to the experimental decrease in binding to 78%.

We also performed MD simulations to compare TM domain changes when CPE did not bind to 5-HTR1E. Figure 2D compares the structures for CPE binding with CPE not bound to 5-HTR1E. When CPE does not bind to the receptor, TM3 and ECL2 move away compared with the CPE bound case, which leads to TM6 movement. Notably, when CPE is absent, the predicted binding free energy of β-arrestin 1 decreases
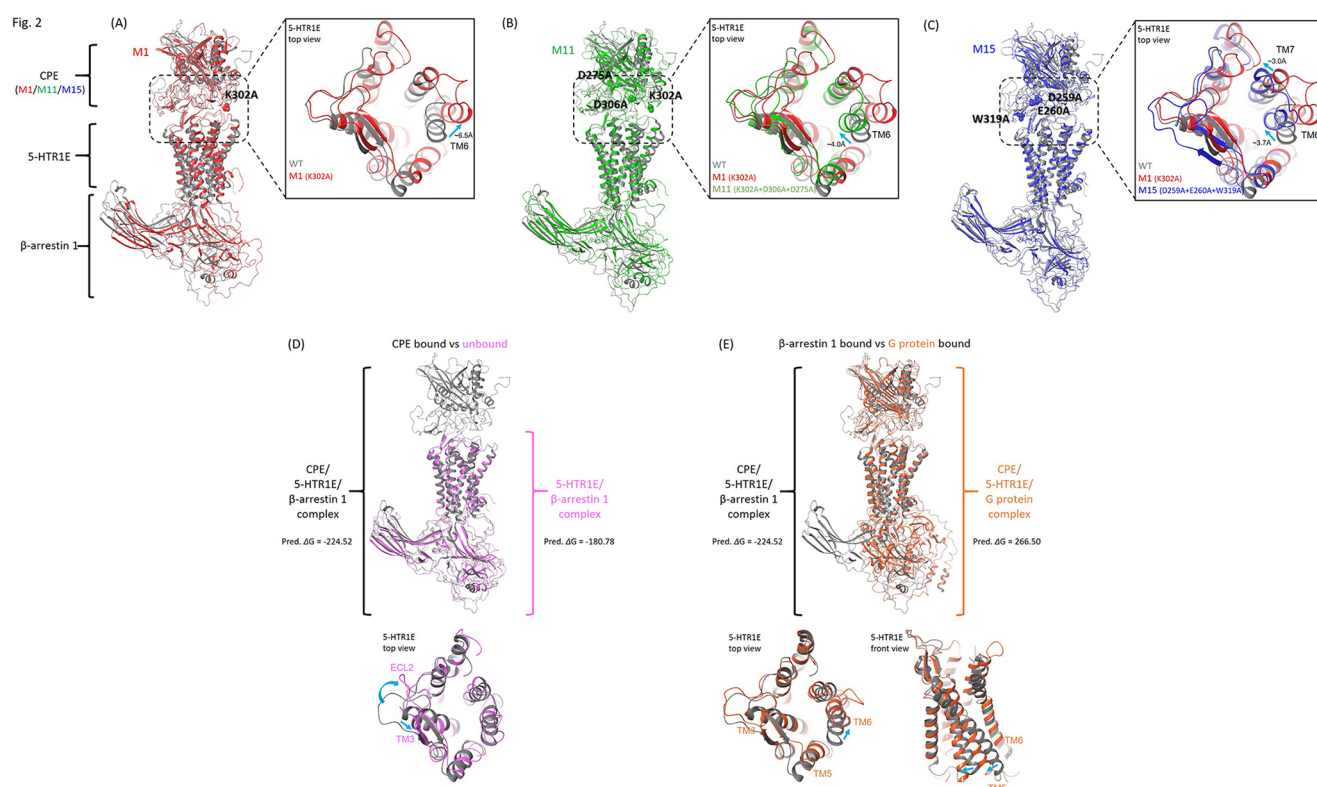
Figure 2. Predicted structural differences between the extracellular domain region of the 5-HTR1E after binding the CPE mutants. (A) The M1 (K302A) CPE mutant compared to WT. The cyan arrow shows the significant movement (6.5 Å) of the TM6 of the 5-HTR1E induced by the K302A mutation in the CPE, (B) the M11 (K302A + D306A + D275A) CPE mutant (M11) compared to M1 (K302A) and WT. This shows the 4.0 Å movement of the TM6 of the 5-HTR1E induced by the mutation in the CPE, and (C) the M15 (D259A + E260A + W319A) CPE mutant compared to M1 (K302A) and WT. This shows the 3.7 Å movement of TM6 and the 3.0 Å movement of TM7 of the 5-HTR1E induced by the mutation in the CPE. (D) The predicted structural differences of the unbound CPE model compared to the bound CPE model of WT. This shows the movement of TM3 and ECL2 of the 5-HTR1E in the absence CPE. (E) The predicted model of binding to a G protein instead of β-arrestin 1.

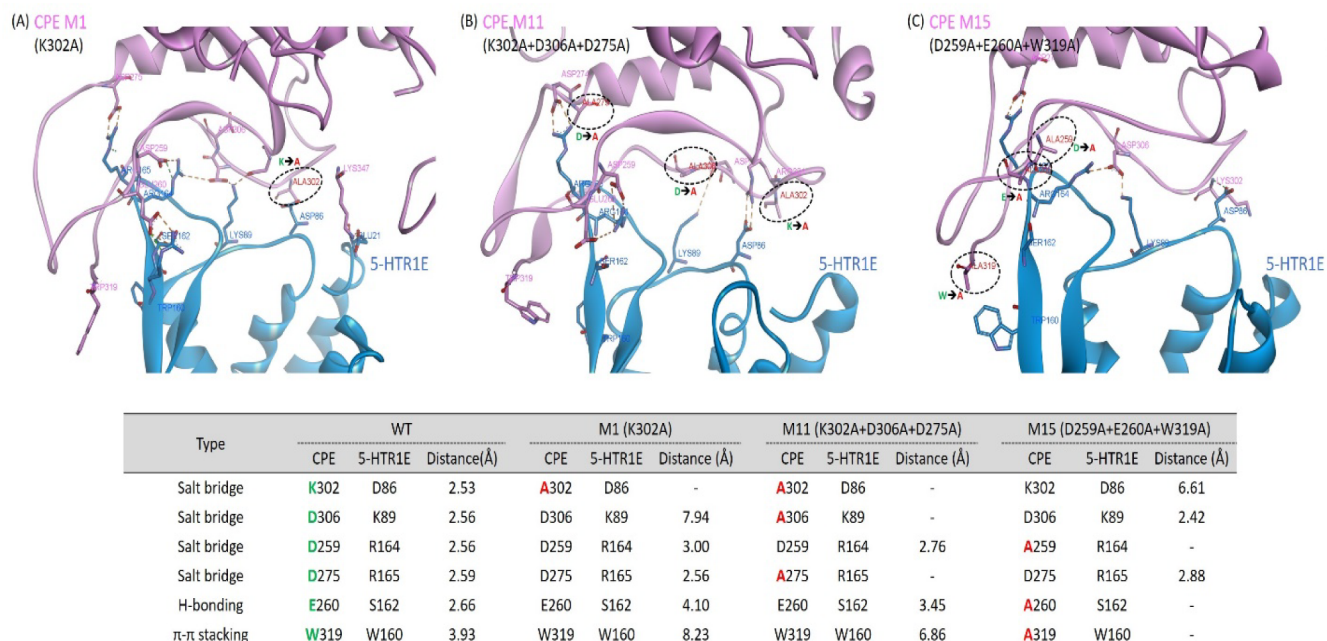| Type	WT			M1 (K302A)			M11 (K302A+D306A+D275A)			M15 (D259A+E260A+W319A)		
	CPE	5-HTR1E	Distance(Å)	CPE	5-HTR1E	Distance (Å)	CPE	5-HTR1E	Distance (Å)	CPE	5-HTR1E	Distance (Å)
Salt bridge	K302	D86	2.53	A302	D86	-	A302	D86	-	K302	D86	6.61
Salt bridge	D306	K89	2.56	D306	K89	7.94	A306	K89	-	D306	K89	2.42
Salt bridge	D259	R164	2.56	D259	R164	3.00	D259	R164	2.76	A259	R164	-
Salt bridge	D275	R165	2.59	D275	R165	2.56	A275	R165	-	D275	R165	2.88
H-bonding	E260	S162	2.66	E260	S162	4.10	E260	S162	3.45	A260	S162	-
π-π stacking	W319	W160	3.93	W319	W160	8.23	W319	W160	6.86	A319	W160	-

Figure 3. Predicted structural details of the binding interface between CPE mutants and 5-HTR1E, showing the hot-spot residues involved the protein−protein interaction. (A) CPE M1 (K302A), (B) CPE M11 (K302A + D306A + D275A), and (C) CPE M15 (D259A + E260A + W319A).

dramatically ($\Delta G = -180.78$) from that in the case with CPE bound to the receptor ($\Delta G = -224.52$). This indicates that

when CPE binds to the 5-HTR1E, the conformational changes of ECL2 and TM6 are important. In addition to β-arrestin 1,

the G protein can also bind to 5-HTR1E when the ligand is present. We conducted MD simulations on whether CPE can recruit the G protein when it binds to the receptor. Figure 2E shows the predicted complex model of the G protein compared to β-arrestin 1. According to our results, when CPE recruits the G protein, there are movements of TM3, TM5, and TM6 of 5-HTR1E compared to β-arrestin 1 binding. The predicted binding free energy of G protein when CPE is present changes by $\Delta G = 266.50$ compared to β-arrestin 1, $\Delta G = -224.52$. This indicates that CPE prefers to recruit β-arrestin 1 rather than the G protein.

Summarizing, our MD simulations led to predicted binding affinities of CPE mutants bound to 5-HTR1E that correlate well with the *in vitro* relative luciferase binding activities. These computations agree with the experiment, in showing that of the mutations we have tested, K302 of CPE is the most important residue for the binding to 5-HTR1E. The movement of TM6 away from TM5 in the extracellular region leads to a compression of intracellular loop 3 (ICL3) that impedes binding and activation of β-arrestin 1.

Figure 3A compares atomic-level details of the salt bridges and their corresponding distances between CPE and the 5-HTR1E complex for WT to that of M1 (K302A). Indeed, the mutation of residue 302 from Lys to Ala breaks the two salt bridges involved in the binding interface between CPE and 5-HTR1E along with the hydrogen bonds to K302. In CPE M1 (K302A), the salt bridge to D86 (in 5-HTR1E) is not formed. Interestingly, the salt bridge between D306 (in CPE) and K89 (in 5-HTR1E) also broke for mutation M1 (K302A). Compared to WT, the M1 (K302A) mutation also lost the hydrogen bond between E260 and S162. Moreover, the $\pi-\pi$ stacking interaction between two Trp rings (W319 in CPE−W160 in 5-HTR1E) does not form.

Figure 3B compares atomic-level details of the interactions and distances at the binding interface between CPE and 5-HTR1E for WT with that of triple combination mutant M11 (K302A + D306A + D275A). Both of the salt bridges between K302A (in CPE) and D86 (in 5-HTR1E) and between D306A (in CPE) and K89 (in 5-HTR1E) present in WT were broken. The hydrogen bonding between E260 and S162 is also lost, and the $\pi-\pi$ stacking interaction between two Trp rings (W319 in CPE−W160 in 5-HTR1E) did not form during MD simulations.

Figure 3C compares atomic-level details of the interactions and their corresponding distance of binding interface between CPE and 5-HTR1E for WT with that of M15 (D259A + E260A + W319A). In this triple mutant, K302 is not mutated. Surprisingly, despite the presence of K302 of WT, the salt bridge between K302 (in CPE) and D86 (in 5-HTR1E) breaks during the MD simulations. As would be expected, the salt bridge between D259A (in CPE) and R164 (in 5-HTR1E) was broken, and the hydrogen bond between E260A (in CPE) and S162 (in 5-HTR1E) does not form. Moreover, the $\pi-\pi$ stacking interaction between W319A (in CPE) and W160 (in 5-HTR1E) does not form due to the mutation.

Surprisingly, all three mutations, M1 (K302A), M11 (K302A + D306A + D275A), and M15 (D259A + E260A + W319A), lead to very similar disruptions in the salt bridges, hydrogen bonds, and $\pi-\pi$ stacking interactions present in WT, with predicted decreases in binding energy similar to experiment. Thus, our MD simulations confirm the decrease in binding observed experimentally, validating the predicted binding site between CPE and 5-HTR1E. Therefore, we conclude that the K302 in CPE is critical for binding to the 5-HTR1E, and it also affects the β-arrestin 1 activation.

Mutation of CPE at K302 + D306A + D275A + D259A + E260A + W319A Together (M16) or K302 Alone (M1) Attenuates Its Ability to Protect Cells from H_2O_2-Induced Cytotoxicity.

Aside from its enzymatic activity involved in hormone maturation, CPE has been found to possess potent extracellular neurotrophic effects.[5,67] A previous study showed that CPE can protect 5-HTR1E expressing cells against H_2O_2-induced cytotoxicity.[11] To test whether the sites mediating the interaction with 5-HTR1E affect CPE's ability to protect cells from stress induced cytotoxicity, we expressed these CPE mutants in HEK293 cells stably transfected with 5-HTR1E and challenged the transfected cells with H_2O_2. As shown in Figure 4, two CPE mutants (M1 and M16)
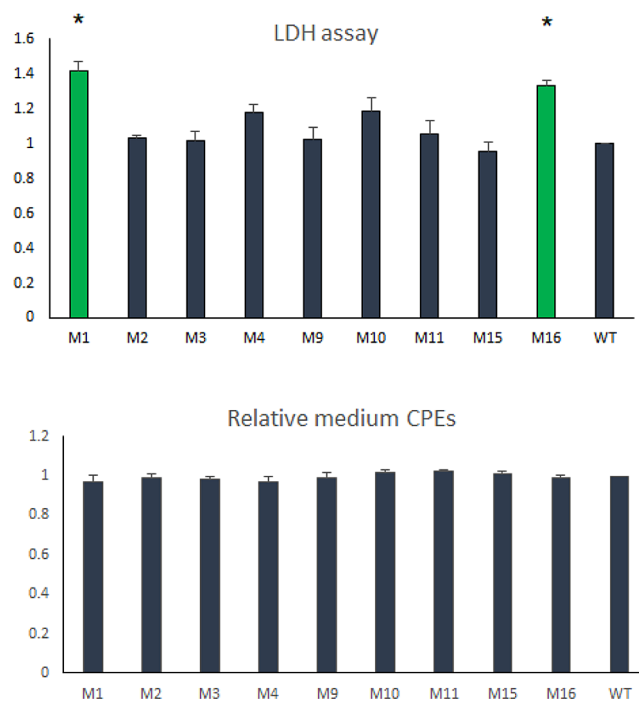

Figure 4. CPE M1 and M16 mutants attenuate CPE's ability to protect cells from H_2O_2-induced cytotoxicity. Upper panel: 5-HTR1E stable HEK293 cells were transfected with each of the CPE mutants as indicated. 48 h after transfection, these cells were challenged with 500 μM H_2O_2 for 4 h, then the LDH activity was measured using cell medium after centrifugation. The bar graph shows the relative cytotoxicity calculated against WT-CPE transfected cells. The Student's t-test was used for statistical analysis. Values are mean ± SD ($N = 3$). *$p < 0.05$. Lower panel: the bar graph shows the relative amount of each CPE mutant against WT-CPE in the medium. No significant difference was observed. Mutants: M1: K302A, M2: D259A, M3: D259N, M4: D275A, M9: E260Q, M10: W319A, M11: K302A + D306A + D275A, M15: D259A + E260A + W319A, M16: K302A + D306A + D275A + D259A + E260A + W319A.

significantly increased cytotoxicity, as tested by the LDH release assay, while the other mutants showed no significant effect. Functionally, the LDH assay reflects CPE's ability to protect cells against stress induced by the H_2O_2 challenge. These results suggest that mutation K302A alone or in combination impairs this protective effect. While mutant M16 harbors all the individual mutations, it showed only a similar cytotoxicity effect as the single mutation M1, which
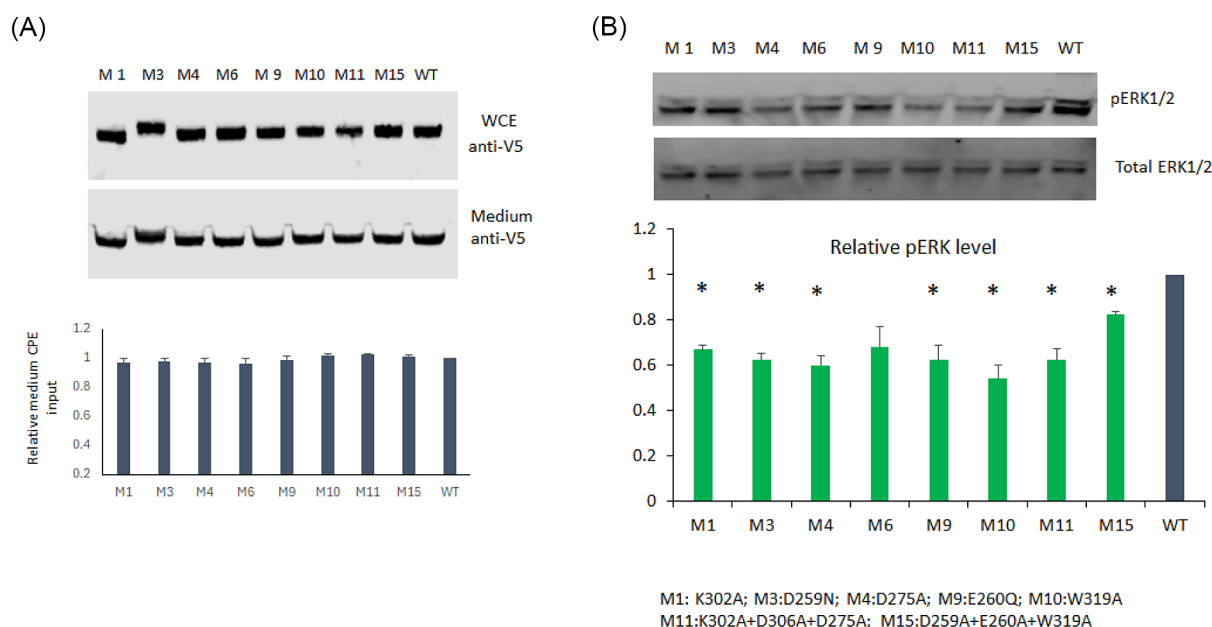
Figure 5. ERK phosphorylation was inhibited by several CPE mutants. 5-HTR1E stable HEK293 cells were treated with the medium obtained from CPE mutant or WT-CPE transfected cells for 5 min. Cells were harvested, lysed, and the pERK1/2 level was analyzed. (A) (upper panel) Representative Western blot analysis of WT-CPE and CPE mutant expression in whole cell lysates of the transfected cell (WCE) and in the secreted medium; (lower panel) the bar graph shows the relative amount of each CPE mutant against WT-CPE in the medium; (B) (upper panel) representative Western blot analysis of pERK1/2 and tERK levels in HTR1E stable HEK293 cells treated with the medium obtained from CPE mutant or WT-CPE transfected cells; (lower panel) the bar graph shows the pERK1/2/total−ERK1/2 ratio relative to the pERK/total ERK ratio in WT-CPE treated HTR1E stable HEK293 cells. The Student's t-test was used for statistical analysis. Values are mean $\pm$ SD ($N = 3$). *$p < 0.05$. Mutants: M1, K302A, M3: D259N, M4: D275A, M6: D306A, M9: E260Q, M10: W319A, M11: K302A + D306A + D275A, M15: D259A + E260A + W319A.

Table 2. Predicted Binding Free Energy of β-Arrestin 1 Based on the MD by MM-GBSA in Complex with 5-HTR1E−CPE Mutants and the Predicted Twist Angle (Small Angle → Lower Activation)[a]

	mutation	predicted ΔG of β-arrestin 1 binding	ratio of predicted ΔG binding	predicted twist angle of β-arrestin 1 (deg)	experimental ratio of pERK level (SEM)[b]
WT		−224.52	1.00	18°[9]	1.00
M15	D259A + E260A + W319A	−211.96	0.94	15°	0.82 ± 0.02
M1	K302A	−189.32	0.84	13°	0.67 ± 0.02
M11	K302A + D306A + D275A	−195.36	0.87	13°	0.62 ± 0.05

[a]Comparison to experimental ratio of pERK level (larger → more activation). [b]Results are expressed as mean ± SEM for each mutant.

corroborates our binding affinity test that site K302 plays an important role in the CPE−5-HTR1E interaction.

Mutation of Specific Amino Acids of CPE Attenuates Its Ability to Activate ERK Phosphorylation. Next, we tested the ERK phosphorylation status of the stable 5-HTR1E cells treated with CPE mutants, since NF-α1/CPE has been shown to protect human hippocampal neurons against H$_2$O$_2$-induced oxidative stress through activation of the ERK signaling pathway.[11] Consistent with previous reports, WT-CPE increased ERK phosphorylation compared with the control (Figure S2). We then transfected eight selected mutant CPE plasmids into stable 5-HTR1E-HEK293 cells and collected the medium of transfected cells to treat untransfected stable 5-HTR1E cells. Western blotting analysis showed that WT-CPE and each of the mutants are efficiently expressed and secreted similarly into the medium of these stable 5-HTR1E cells (Figure 5A). As shown in Figure 5B, a decreased pERK1/2 level was observed with CPE bearing mutations at single sites, M1 (K302A), M3 (D259N), M4 (D275A), M9 (E260Q), M10 (W391A) and a combination of mutations at

M11 (K302A + D306A + D275A) and M15 (D259A + E260A + W319A), as compared with WT-CPE ($p < 0.05$). Other CPE single amino acid mutations showed no statistically significant effect on ERK phosphorylation but lower pERK1/2 levels. These results indicate that most mutants decreased pERK1/2 levels in 5-HTR1E-HEK293 cells when compared with WT-CPE, which is consistent with the lower binding affinity caused by these mutations, as shown previously in Figure 1.

Structural Mechanism for CPE Mutation Related to Activate ERK Phosphorylation. To investigate the molecular mechanism regulated through β-arrestin 1 correlation with ERK phosphorylation according to mutation of specific amino acids of CPE, we carried out binding free energy calculations between 5-HTR1E and the β-arrestin 1 complex using MD simulations for three CPE mutants, M1 (K302A), M11 (K302A + D306A + D275A), and M15 (D259A + E260A + W319A). The predicted binding free energy of the β-arrestin 1 complex with 5-HTR1E/CPE mutants is shown in Table 2 and Figure 6. The β-arrestin 1 in WT-CPE strongly binds to the 5-HTR1E, but all three mutants lead to a dramatic decrease in
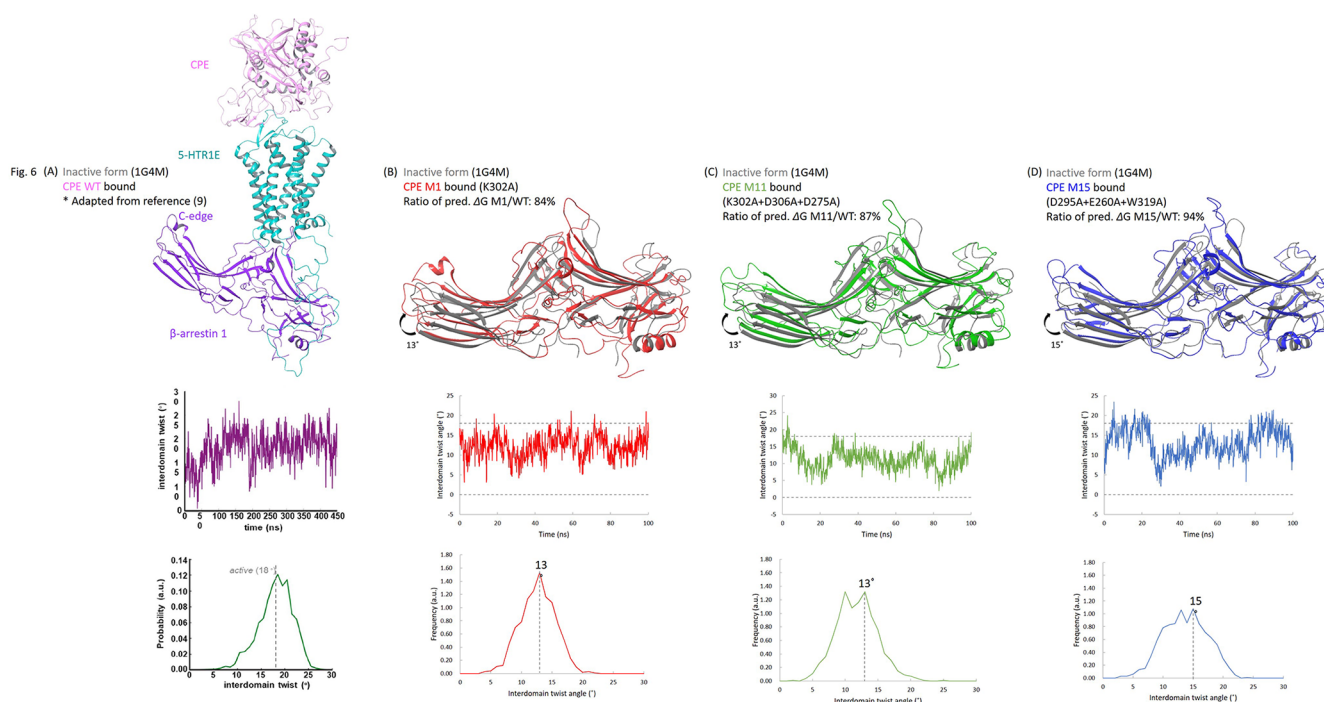
Figure 6. Analysis of the predicted β-arrestin 1 conformation bound to CPE/5-HTR1E complexes including the distribution of the interdomain twist angles of the β-arrestin 1 that indicates level of activation. (A) M1 (K302A) (B) M11 (K302A + D306A + D275A), and (C) M15 (D259A + E260A + W319A) CPE mutants. *The distribution of the interdomain twist angles of the β-arrestin 1 in WT was adapted from ref 9.

binding to 84% of WT for M1 (K302A), to 87% of WT for M11 (K302A + D306A + D275A), and to 94% of WT for M15 (D259A + E260A + W319A), which correlates well with the decreased pERK level (down to 67%, 62%, and 82%, of the WT control, respectively).

We focused on the analysis of the conformational changes at the intracellular loops (ICL1, ICL2, and ICL3) of 5-HTR1E that are involved in the binding to β-arrestin 1. Based on our MD simulation results, when CPE mutants bind to 5-HTR1E, the ICL1 and ICL2 conformations did not change compared to WT CPE. Interestingly, ICL3 in 5-HTR1E showed minor changes in the loop complexed with CPE mutants (Figure S3). The ICL3 flips to the inside for M1 (K302A), M11(K302A + D306A + D275A), and M15 (D259A + E260A + W319A) compared to that of the WT. This finding reveals that minor changes in the structure of the ICL3 of 5-HTR1E can lead to pronounced changes in the β-arrestin 1 binding.

Our previous study[11] showed that binding β-arrestin 1 at WT CPE led to β-arrestin activation with an average interdomain twist angle of ~18°.[2,12,1314] Thus, we now measured the interdomain twist angle in the M1 (K302A), M11 (K302A + D306A + D275A), and M15 (D259A + E260A + W319A) CPE mutants, all of which are between 13° and 15°, much smaller than WT (see Table 2 and Figure 6). Interestingly, the twist angle of M15 (D259A + E260A + W319A) CPE shows the largest twist of ~15°, which correlates with the highest ERK phosphorylation level among three CPE mutants.

These experimental and computational results confirm that mutating CPE residues in the predicted binding site to 5-HTR1E induces decreased binding affinity between CPE and 5-HTR1E and between 5-HTR1E and β-arrestin 1. We found that the conformational changes of mutant CPE/5-HTR1E trigger movements of the extracellular TM6 and EC3 loops

away from the TM5 in 5-HTR1E, which in turn weakens the binding of β-arrestin 1 to ICL3 that decreases the activation of β-arrestin 1.

■ SUMMARY AND CONCLUSION

Our experimental tests of the binding of mutant CPE to 5-HTR1E identified three mutants with clearly decreased binding. These same three mutants also led to dramatically decreased pERK levels. These results confirm the previously predicted CPE binding site.

We then followed up with MD simulations of these three mutants and found decreases in the level of binding of CPE to 5-HTR1E for all three, in excellent agreement with our experiments. Our detailed atomistic-level analysis of the binding site for the mutants found that all three mutants lead to similar disruptions in the salt bridges, hydrogen bonds, and $\pi-\pi$ stacking interactions of CPE with 5-HTR1E despite the differences in the specific mutation patterns.

We then examined computationally the activation of β-arrestin by the three mutants and found that all three led to a dramatic decrease in binding, as observed experimentally by pERK measurements, as well as decreased β-arrestin activation, as measured by the decrease in twist angle.

This strong agreement of the new MD with the new experiments and the strong agreement of the new experiments with the previously predicted binding site provide very strong affirmation of the CPE binding site to 5-HTR1E responsible for β-arrestin activation and subsequent neuro protection.

This sets the stage for seeking small molecules that can bind to the same pharmacophore. We plan now to carry out *in silico* searches for small ligands that bind to the same site, which will be followed by experimental tests. Hopefully, this will identify prime molecules that will eventually lead to new drugs that can

protect human neurons against oxidative/neuroexcitotoxic stress via β-arrestin/ERK signaling.

■ MATERIALS AND METHODS

DNA Constructs. Plasmids expressing human wild type (WT) and mutant CPE with C-terminal V5 tag were constructed into the pcDNA 3.1 backbone by GenScript (GenScript, NJ, USA) as follows: M1: K302A, M2: D259A, M3: D259N, M4: D275A, M5: D275N, M6: D306A, M7: D306N, M8: 260A, M9: E260Q, M10: W319A, M11: K302A + D306A + D275A, M12: D259A + E260A, M13: K302A + D259A + E260A, M14: K302A + D306A + W319A, M15: D259A + E260A + W319A, M16: K302A + D306A + D275A + D259A + E260A + W319A. Plasmid expressing human 5-HTR1E with a C-terminal Myc tag was purchased from Origene (Rockville, MD).

Western Blot. Cells were lysed in RIPA buffer (cat. no. 89901, Thermo Scientific, USA) containing proteinase inhibitor or phosphatase inhibitor (for phosphorylation test). Proteins were quantified using BCA or Bradford assay and separated on SDS-PAGE gel, followed by Western blotting and probed with antibody. Protein bands were visualized with the Odyssey infrared imaging system and software (LI-COR Inc., Lincoln, NE).

Luciferase Assay. The Presto-Tango luciferase reporter system was used to test the binding affinity as previously reported[11] with modification. Briefly, 5-HTR1E and Renilla luciferase plasmids were cotransfected along with each of the 16 CPE mutants and WT-CPE plasmids into HTLA cells (an HEK293 cell line stably expressing a combination of a tTA-dependent luciferase reporter and a β-arrestin 2-TEV fusion gene.[15] HTLA cells were transfected in 96 or 12 well plates at a density of 10,000/100,000 cells per well in DMEM supplemented with 10% FBS; next day 0.2 μg of 5-HTR1E, 0.2 μg of CPE mutant, and 0.05 μg of Renilla luciferase plasmids were cotransfected cells in a 96 well plate by using Lipofectamine 2000 (DNA/Lipofectamine 2000 ratio is 1:3) in OPTI-MEM transfection medium according to the manufacturer's manual. For 12-well plate transfection, 1 μg of 5-HTR1E and 1 μg of CPE mutant were cotransfected by using Lipofectamine 2000 (DNA/Lipofectamine 2000 ratio is 1:3) in OPTI-MEM transfection medium, according to the manufacturer's manual. Renilla luciferase or Western blotting was used to evaluate CPE mutants' expression efficacy. WT-CPE plasmid and empty pcDNA3.1 vector served as positive and negative controls, respectively. After 48 h, transfected cells were lysed for luciferase assay using a dual luciferase system (Promega) according to the manual's instruction. Luminescence was measured using a Synergy HTX plate reader (Biotech, USA).

Lactate Dehydrogenase (LDH) Cytotoxicity Assay. The LDH assay was carried out using a CytoTox 96 Non-Radioactive Cytotoxicity Assay kit (Promega, cat. no. G1780) to measure the release of LDH from damaged cells. Briefly, 3 × 10^5 of 5-HTR1E stable HEK293 cells were seeded into 12-well plate overnight; the next day, 2 μg of CPE or CPE mutant plasmid was transfected into the cells using Lipofectamine 2000 (Thermo Fisher, Cat# 11668019) according to manufacturer's instructions. 48 h after transfection, 1 × 10^4 of transfected cells were reseeded into a 96 well plate overnight; the next day, the regular DMEM medium was removed and cells were treated with 200 μL of serum free DMEM medium containing 500 μM H_2O_2 for 4 h. 50 μL of

debris-free medium was collected for the LDH assay. A Biotek microplate reader was used to read absorbance at 490 nm, and relative cytotoxicity was calculated against control cells.

ERK Activation Assay. 5-HTR1E stable HEK293 cells were seeded in a 12-well plate at 70% confluency in DMEM supplemented with 10% FBS and incubated at 37 °C in a CO_2 incubator overnight. Next day, plasmids expressing WT-CPE or each of the CPE mutants were transfected into the 5-HTR1E stable cells using Lipofectamine 2000 according to manual's instruction. 48 h after transfection, the cells were starved in serum free DMEM for 12 h, and then 1 mL of medium containing secreted CPE or mutant CPE was collected and centrifuged at 5000 rpm for 5 min to remove cell debris. For ERK phosphorylation assay, 5-HTR1E stable HEK293 cells were seeded in 12-well plate at 70% confluency in DMEM supplemented with 10% FBS and incubated overnight at 37 °C in a CO_2 incubator. The next day, the cell medium was replaced with the medium collected previously from transfected cells and incubated for 5 min. Then, the cells were collected and lysed, and the lysates were used for the ERK phosphorylation assay by Western blotting. The level of pERK was assessed by using phosphorylated ERK (pERK1/2) (T202/Y204) rabbit antibody and total ERK (tERK1/2) mouse monoclonal antibody simultaneously. An Odyssey fluorescence scanner was used to visualize the protein bands. Phosphorylated ERK was normalized against total ERK, and fold changes were calculated from three independent experiments after densitometric analysis using ImageJ software, NIH.

CPE Mutant Model Generation. We started with our GEnSeMBLE (GPCR Ensemble of Structures in Membrane BiLayer Environment)[15−19] predicted structure for the WT model 5HTR1E attached to Gi protein and the CPE protein fragment that was equilibrated for 0.7 μs of MD simulation at 310 K. Then, we made the following mutations and equilibrated:

- K302−D86 (ECL1),
- D306−K89 (ECL1),
- D275−R165 (ECL2),
- D259−R164 (ECL2),
- E260−S162 (ECL2), and
- W319−W160 (ECL2).

The CPE/5-HTR1/β-arrestin 1 complex models for the 8 mutants (M1: K302A, M3: D259N, M4: D275A, M6: D306A, M9: E260Q, M10: W319A, M11: K302A + D206A + D275A, and M15: D259A + E260A + W319A) were retrieved from the published WT model with our GEnSeMBLE. The 8 mutant models were built using the Mutate Residues Wizard, and we minimized side chains using the Maestro v13.3 of Schrödinger Suite 2022-3 (Schrödinger, LLC, New York, NY, USA, 2022).

Molecular Dynamics (MD) Simulations. The molecular dynamics (MD) simulations with explicit solvent were performed using Desmond version 7.1 with the OPLS_2005 force field (Schrödinger Release 2022-3: Desmond Molecular Dynamics System, D. E. Shaw Research: New York, NY, 2022). The OPM (Orientations of Proteins in Membranes)[20] database was used for the spatial arrangement of the protein structures in lipid bilayers. The human 5-HTR1E complex with Gi protein (PDB ID 7E33) Cryo-EM structure[21] was downloaded from the OPM database (https://opm.phar.umich.edu). Then, the 8 mutant models were superimposed to the 5-HTR1E Cryo-EM structure preoriented with respect

to the membrane model. We selected the POPC (1-palmytoyl-2-oleoyl-*sn*-glycero-3-phosphatidylcholine) bilayer model for the membrane, where the membrane position was aligned according to the structure obtained from the OPM database in the System Builder of Desmond. The thickness of the membrane model in Cryo-EM 5-HTR1E was set to 32.2. TIP3P[21,22] water was selected as the solvent model using an orthorhombic box with dimensions of 10 Å × 20 Å × 10 Å. The overall complex structure was neutralized by adding Cl⁻ counterions. Then, the NaCl salt concentration was adjusted to 0.15 mol/L. Then, MD simulations of length 100 ns were carried out with periodic boundary conditions using the *NPT* ensemble at body temperature (310 K) and pressure (1.01325 bar) for relaxation before simulation. The Nose−Hoover chain thermostat algorithm[23−26] and Martyna−Tobias−Klein barostat[27] were utilized to maintain the temperature and pressure, respectively. The RESPA integrator[28] was used with a time step of 2 fs during the simulation using a smooth PME method for the calculation of long-range electrostatic interaction. Recording intervals of 1.2 and 100 ps were used for energy calculation and trajectory analysis. The analyzed protein interface and proposed interaction model of the equilibrium state of the 8 CPE mutant/5-HTR1E/β-arrestin1 complex structures were represented using Discovery Studio 2022 (Dassault Systems BIOVIA, San Diego, CA, USA, 2022).

Molecular Mechanics-Generalized Born Surface Area (MM-GBSA) Calculation. The final equilibrium state for protein−protein docking poses was rescored with the MM-GBSA[29,28] approach, as implemented in the Prime MM-GBSA module in the Schrödinger Suite 2022-3. We used the OPLS_2005 force field, the VSGB solvation model, and the default Prime parameters for the MM-GBSA calculations. The binding free energy was calculated for 20 frames based on the last 100 ns MD trajectory for each mutant.

Statistical Analysis. Data are representative of triplicates for each experiment and at least 3 separate experiments (*N*). The data were analyzed by a two-tailed Student's *t*-test. Statistical significance was defined as $p < 0.05$.

■ ASSOCIATED CONTENT

Data Availability Statement
All data sets generated and/or analyzed during the current study are available from the corresponding authors upon reasonable request.

Ⓢ Supporting Information
The Supporting Information is available free of charge at https://pubs.acs.org/doi/10.1021/acsomega.4c05367.

> Methods and materials, HTLA cells transfected with plasmids expressing WT-CPE or each of the CPE mutants; Western blot analysis of pERK1/2 and tERK levels in HTR1E stable HEK293 cells treated with the medium obtained from CPE or vector transfected cells; structural analysis of intracellular loops (ICL1, ICL2, and ICL3) of 5-HTR1E upon CPE mutant binding. rmsd plots for eight CPE mutants/5-HTR1E/β-arrestin 1 complex of 100 ns MD simulations (PDF)

■ AUTHOR INFORMATION

Corresponding Authors
William A. Goddard, III − *Materials and Process Simulation Center, California Institute of Technology, Pasedena, California 91125, United States;* ● orcid.org/0000-0003-0097-5716; Email: wag@caltech.edu

Y. Peng Loh − *Section on Cellular Neurobiology, Eunice Kennedy Shriver National Institute of Child Health and Human Development, National Institutes of Health, Bethesda, Maryland 20892, United States;* Phone: (301) 4963239; Email: lohp@mail.nih.gov

Authors
Xuyu Yang − *Section on Cellular Neurobiology, Eunice Kennedy Shriver National Institute of Child Health and Human Development, National Institutes of Health, Bethesda, Maryland 20892, United States*

Joo-Youn Lee − *Materials and Process Simulation Center, California Institute of Technology, Pasedena, California 91125, United States; Therapeutics and Biotechnology Division, Korea Research Institute of Chemical Technology, Daejeon 34114, Republic of Korea;* ● orcid.org/0000-0001-5685-9875

Soo-Kyung Kim − *Materials and Process Simulation Center, California Institute of Technology, Pasedena, California 91125, United States*

Complete contact information is available at:
https://pubs.acs.org/10.1021/acsomega.4c05367

■ ACKNOWLEDGMENTS

■ ABBREVIATIONS

5-HTR1E, serotonin receptor 1E
AAV, adeno-associated virus
BDNF, brain-derived neurotrophic factor
CPE, carboxypeptidase E
Cryo-EM, cryogenic electron microscopy
DMEM, Dulbecco's modified Eagle medium
ECL, extracellular loops
EGF, epidermal growth factor
ERK, extracellular signal-regulated kinase

FGF, fibroblast growth factor 2

GEnSeMBLE, GPCR ensemble of structures in membrane bilayer environment

GPCR, G protein-coupled receptor

HTLA, an HEK293 cell line stably expressing a tTA-dependent luciferase reporter and a β-arrestin2-TEV fusion gene

HTR1E, serotonin receptor 1E

ICL, intracellular loop

IGFs, insulin-like growth factor

LDH, lactate dehydrogenase

MD, molecular dynamics

MM-GBSA, molecular mechanics, generalized Born surface area

NF-α1, neurotrophic factor-α1

OPLS, optimized potentials for liquid simulations

OPM, orientations of proteins in membranes

PDB:, protein data bank

PME, particle mesh Ewald

POPC, 1-palmytoyl-2-oleoyl-*sn*-glycero-3-phosphatidylcholine

RESPA, reversible reference system propagator algorithms

TGFs, transforming growth factors

TM, transmembrane domain

TIP3P, transferable intermolecular potential with 3 points

WT, wild type

■ REFERENCES

(1) Vassar, R.; Zheng, H. Molecular neurodegeneration: basic biology and disease pathways. *Mol. Neurodegener.* 2014, 9, 34.

(2) Zhou, X. E.; He, Y.; de Waal, P. W.; Gao, X.; Kang, Y.; Van Eps, N.; Yin, Y.; Pal, K.; Goswami, D.; White, T. A.; Barty, A.; et al. Identification of Phosphorylation Codes for Arrestin Recruitment by G Protein-Coupled Receptors. *Cell* 2017, 170 (3), 457−469.e13.

(3) Lyons, R. M.; Moses, H. L. Transforming growth factors and the regulation of cell proliferation. *Eur. J. Biochem.* 1990, 187 (3), 467−473.

(4) Radin, D. P.; Patel, P. BDNF: An Oncogene or Tumor Suppressor? *Anticancer Res.* 2017, 37 (8), 3983−3990.

(5) Cheng, Y.; Cawley, N. X.; Loh, Y. P. Carboxypeptidase E/NFalpha1: a new neurotrophic factor against oxidative stress-induced apoptotic cell death mediated by ERK and PI3-K/AKT pathways. *PLoS One* 2013, 8 (8), No. e71578.

(6) Xiao, L.; Yang, X.; Loh, Y. P. Neurotrophic, Gene Regulation, and Cognitive Functions of Carboxypeptidase E-Neurotrophic Factor-alpha1 and Its Variants. *Front. Neurosci.* 2019, 13, 243.

(7) Xiao, L.; Sharma, V. K.; Toulabi, L.; Yang, X.; Lee, C.; Abebe, D.; Peltekian, A.; Arnaoutova, I.; Lou, H.; Loh, Y. P.; et al. Neurotrophic factor-α1, a novel tropin is critical for the prevention of stress-induced hippocampal CA3 cell death and cognitive dysfunction in mice: comparison to BDNF. *Transl. Psychiatry* 2021, 11 (1), 24.

(8) Xiao, L.; Yang, X.; Sharma, V. K.; Abebe, D.; Loh, Y. P. Hippocampal delivery of neurotrophic factor-alpha1/carboxypeptidase E gene prevents neurodegeneration, amyloidosis, memory loss in Alzheimer's Disease male mice. *Mol. Psychiatry* 2023, 28 (8), 3332−3342.

(9) Jiang, D.; Liu, H.; Li, T.; Zhao, S.; Yang, K.; Yao, F.; et al. Agomirs upregulating carboxypeptidase E expression rescue hippocampal neurogenesis and memory deficits in Alzheimer's disease. *Transl. Neurodegener.* 2024, 13 (1), 24.

(10) Bai, F.; Yin, T.; Johnstone, E. M.; Su, C.; Varga, G.; Little, S. P.; Nelson, D. L.; et al. Molecular cloning and pharmacological characterization of the guinea pig 5-HT1E receptor. *Eur. J. Pharmacol.* 2004, 484 (2−3), 127−139.

(11) Sharma, V. K.; Yang, X.; Kim, S. K.; Mafi, A.; Saiz-Sanchez, D.; Villanueva-Anguita, P.; Xiao, L.; Toulabi, L.; Inoue, A.; Goddard, W. A.; Loh, Y. P.; et al. Novel interaction between neurotrophic factor-α1/carboxypeptidase E and serotonin receptor, 5-HTR1E, protects human neurons against oxidative/neuroexcitotoxic stress via β-arrestin/ERK signaling. *Cell. Mol. Life Sci.* 2022, 79 (1), 24.

(12) Latorraca, N. R.; Wang, J. K.; Bauer, B.; Townshend, R. J. L.; Hollingsworth, S. A.; Olivieri, J. E.; Xu, H. E.; Sommer, M. E.; Dror, R. O.; et al. Molecular mechanism of GPCR-mediated arrestin activation. *Nature* 2018, 557 (7705), 452−456.

(13) Shukla, A. K.; Manglik, A.; Kruse, A. C.; Xiao, K.; Reis, R. I.; Tseng, W. C.; Staus, D. P.; Hilger, D.; Uysal, S.; Huang, L.-Y.; Paduch, M.; et al. Structure of active β-arrestin-1 bound to a G-protein-coupled receptor phosphopeptide. *Nature* 2013, 497 (7447), 137−141.

(14) Chen, Q.; Perry, N. A.; Vishnivetskiy, S. A.; Berndt, S.; Gilbert, N. C.; Zhuo, Y.; et al. Structural basis of arrestin-3 activation and signaling. *Nat. Commun.* 2017, 8 (1), 1427.

(15) Barnea, G.; Strapps, W.; Herrada, G.; Berman, Y.; Ong, J.; Kloss, B.; Axel, R.; Lee, K. J.; et al. The genetic design of signaling cascades to record receptor activation. *Proc. Natl. Acad. Sci. U. S. A.* 2008, 105 (1), 64−69.

(16) Abrol, R.; Kim, S.-K.; Bray, J. K.; Trzaskowski, B.; Goddard, W. A., III Conformational ensemble view of G protein-coupled receptors and the effect of mutations and ligand binding. *Methods Enzymol.* 2013, 520, 31−48.

(17) Abrol, R.; Bray, J. K.; Goddard, W. A., III Bihelix: Towards de novo structure prediction of an ensemble of G-protein coupled receptor conformations. *Proteins* 2012, 80 (2), 505−518.

(18) Abrol, R.; Griffith, A. R.; Bray, J. K.; Goddard, W. A., III Structure prediction of G protein-coupled receptors and their ensemble of functionally important conformations. *Methods Mol. Biol.* 2012, 914, 237−254.

(19) Bray, J. K.; Abrol, R.; Goddard, W. A., III; Trzaskowski, B.; Scott, C. E. SuperBiHelix method for predicting the pleiotropic ensemble of G-protein-coupled receptor conformations. *Proc. Natl. Acad. Sci. U. S. A.* 2014, 111 (1), No. E72−8.

(20) Lomize, M. A.; Lomize, A. L.; Pogozheva, I. D.; Mosberg, H. I. OPM: orientations of proteins in membranes database. *Bioinformatics* 2006, 22 (5), 623−625.

(21) Xu, P.; Huang, S.; Zhang, H.; Mao, C.; Zhou, X. E.; Cheng, X.; Simon, I. A.; Shen, D.-D.; Yen, H.-Y.; Robinson, C. V.; Harpsøe, K.; et al. Structural insights into the lipid and ligand regulation of serotonin receptors. *Nature.* 2021, 592 (7854), 469−473.

(22) Jorgensen, W. L.; Chandrasekhar, J.; Madura, J. D.; Impey, R. W.; Klein, M. L. Comparison of Simple Potential Functions for Simulating Liquid Water. *J. Chem. Phys.* 1983, 79 (2), 926−935.

(23) Nose, S. A Unified Formulation of the Constant Temperature Molecular-Dynamics Methods. *J. Chem. Phys.* 1984, 81 (1), 511−519.

(24) Nose, S. A Molecular-Dynamics Method for Simulations in the Canonical Ensemble. *Mol. Phys.* 1984, 52 (2), 255−268.

(25) Hoover, W. G. Canonical Dynamics - Equilibrium Phase-Space Distributions. *Phys. Rev. A* 1985, 31 (3), 1695−1697.

(26) Martyna, G. J.; Klein, M. L.; Tuckerman, M. Nose-Hoover Chains - the Canonical Ensemble Via Continuous Dynamics. *J. Chem. Phys.* 1992, 97 (4), 2635−2643.

(27) Martyna, G. J.; Tobias, D. J.; Klein, M. L. Constant-Pressure Molecular-Dynamics Algorithms. *J. Chem. Phys.* 1994, 101 (5), 4177−4189.

(28) Bowers, K. J.; Chow, E.; Xu, H.; Dror, R. O.; Eastwood, M. P.; Gregersen, B. A.; Klepeis, J. L.; Kolossvary, I.; Moraes, M. A.; Sacerdoti, F. D. Scalable algorithms for molecular dynamics simulations on commodity clusters. In *SC'06: Proceedings of the 2006 ACM/IEEE conference on Supercomputing*; IEEE, 2006; p. 84.

(29) Li, J.; Abel, R.; Zhu, K.; Cao, Y.; Zhao, S.; Friesner, R. A. The VSGB 2.0 model: A next generation energy model for high resolution protein structure modeling. *Proteins-Structure Function And Bioinformatics* 2011, 79 (10), 2794−2812.